batteries

MDPI

Article

Toward Circular Carbon: Upcycling Coke Oven Waste into Graphite Anodes for Lithium-Ion Batteries

Seonhui Choi †, Inchan Yang †, Byeongheon Lee, Tae Hun Kim, Sei-Min Park * and Jung-Chul An *

Carbon Materials Research Cell, Research Institute of Industrial Science & Technology (RIST), Pohang 37673, Republic of Korea; hes02427@rist.re.kr (S.C.); iyang@rist.re.kr (I.Y.); leebh1784@rist.re.kr (B.L.); thkim5749@rist.re.kr (T.H.K.)

* Correspondence: smpark1@rist.re.kr (S.-M.P.); jcan@rist.re.kr (J.-C.A.)

† These authors contributed equally to this work.

Abstract

This study presents a sustainable upcycling strategy to convert "Pit," a carbon-rich coke oven by-product from steel manufacturing, into high-purity graphite for use as an anode material in lithium-ion batteries. Despite its high carbon content, raw Pit contains significant impurities and has irregular particle morphology, which limits its direct application in batteries. We employed a multi-step, additive-free refinement process—including jet milling, spheroidization, and high-temperature graphitization—to enhance carbon purity and structural properties. The processed Pit-derived graphite showed a much-improved particle size distribution (D50 reduced from 25.3 μm to 14.8 μm & Span reduced from 1.72 to 1.23), increased tap density (from 0.54 to 0.80 g/cm^3), and reduced BET surface area, making it suitable for high-performance lithium-ion batteries anodes. Structural characterization by XRD and TEM confirmed dramatically enhanced crystallinity after graphitization (graphitization degree increasing from ~13 for raw Pit to 95.7% for graphitized Pit at 3000 °C). The fully processed graphite (denoted S_Pit3000) delivered a reversible discharge capacity of 346.7 mAh/g with an initial Coulombic efficiency of 93.5% in half-cell tests—comparable to commercial artificial graphite. Furthermore, when composited with silicon oxide to form a hybrid anode, the material achieved an even higher capacity of 418.0 mAh/g under high mass loading conditions. These results highlight the feasibility of transforming industrial coke waste into value-added electrode materials through environmentally friendly physical processes. The upcycled graphite anode meets industrial performance standards, demonstrating a promising route toward circular economy solutions in both the steel and battery industries.

Keywords: circular economy; graphite anode; coke oven waste; lithium-ion battery

Academic Editor: Ivana Hasa

Received: 15 August 2025
Revised: 13 September 2025
Accepted: 30 September 2025
Published: 2 October 2025

Citation: Choi, S.; Yang, I.; Lee, B.; Kim, T.H.; Park, S.-M.; An, J.-C. Toward Circular Carbon: Upcycling Coke Oven Waste into Graphite Anodes for Lithium-Ion Batteries. *Batteries* **2025**, *11*, 365. https://doi.org/10.3390/batteries11100365

1. Introduction

The global transition to electric vehicles (EVs) and renewable energy storage has driven a surging demand for lithium-ion batteries (LIBs) and, consequently, for the critical minerals that constitute them [1–5]. Graphite, which serves as the anode in LIBs, is indispensable due to its excellent electrical conductivity, layered structure for Li-ion intercalation, and relatively low cost [6–8]. Nearly all commercial LIBs rely on graphite anodes, and no large-scale substitute has yet emerged to match graphite's combination of performance and stability. LIB demand is projected to multiply in the coming years, with graphite demand expected to grow fourfold by 2030 compared to 2023 [9]. Each EV requires

approximately 70 kg of graphite for its battery, meaning that one million EVs would consume around 70,000 tons of graphite [10,11]. Ensuring a sustainable and resilient supply of such enormous quantities poses a significant challenge.

Unlike lithium or cobalt, graphite is not inherently scarce in the Earth's crust; however, its production is heavily geographically concentrated. Over 70% of the global graphite supply chain is controlled by a single country (China), which also produces over 90% of battery-grade anode materials [12,13]. This concentration creates substantial geopolitical and economic risks for battery manufacturers. As of 2023, China accounted for roughly 77% of natural graphite production and virtually all downstream spheroidized and purified graphite used in anodes. While other countries are accelerating projects to diversify sourcing, significant time and investment are required to achieve supply chain resilience.

The graphite anode industry also faces environmental and economic hurdles. Natural graphite must be purified—often using hydrofluoric acid—and shaped into spherical particles, processes that are chemically intensive and generate hazardous waste. Artificial graphite, produced by graphitizing petroleum coke or other carbon precursors at around 3000 °C, entails a substantial energy demand and a significant carbon footprint. Recent life-cycle assessments show that producing 1 kg of coated spherical graphite in China emits roughly 9–10 kg CO_2-equivalent, and even cleaner processes elsewhere emit 3–7 kg/kg [10]. Artificial graphite is even more carbon-intensive, at ~20–25 kg CO_2 per kg produced [14]. These factors underscore the urgent need for more sustainable and locally sourced anode materials.

In response, there is growing interest in a circular economy strategy for battery materials, wherein end-of-life products and industrial wastes are recycled or upcycled into new battery components. Circular approaches can reduce reliance on virgin raw materials, lower environmental impacts, and improve material security. For graphite anodes, this could involve both recycling spent anodes from used batteries and upcycling other carbon-rich wastes into battery-grade carbons. Graphite is one of the few battery materials that can theoretically be directly recovered and reused with minimal chemical alteration, as carbon does not undergo the phase transformations that cathode metals do during cycling. However, as little as ~5% of spent LIBs are currently recycled, and most recovery efforts have historically focused on valuable metals such as Co, Ni, and Li.

Recent studies have demonstrated that graphite recovered from spent LIB anodes can retain respectable capacity (~300 mAh/g) after mild reconditioning, and simple treatments such as ball milling can enhance its performance to approach that of virgin material [15–17]. Markey et al. achieved "direct regeneration" of degraded graphite anodes through thermal healing and nitrogen doping, restoring electrochemical performance close to baseline [18].

Beyond spent batteries, researchers have explored upcycling non-battery carbon waste streams into new anode materials. Many industrial by-products have high fixed-carbon content but low economic value, making them attractive for valorization. Examples include petroleum coke, coal tar pitch, end-of-life plastics, biomass wastes, and even discarded personal protective equipment such as COVID-19 masks. These feedstocks can be carbonized, activated, or graphitized to produce carbons for energy storage devices [19–23].

For instance, Hong et al. transformed polyolefins into soft carbon anodes delivering ~300 mAh/g via hydrothermal carbonization [24], while Vander Wal et al. graphitized single-use plastic waste using graphenic catalysts to produce high-purity graphite suitable for LIB anodes [25]. Kim et al. combined waste PET plastic with pyrolysis fuel oil pitch to generate graphitizable carbon with nanoporous features that improved Li storage capacity [26]. Additionally, a recent study by Kim et al. examined how heat-treatment temperature and duration influence mesophase pitch development in coal tar pitch, find-

ing that higher temperatures led to increased crystalline order and reduced interlayer spacing—properties beneficial for LIB anodes [27].

In this context, the present study investigates coke oven waste as an alternative carbon feedstock for LIB anodes. Coke ovens, integral to steelmaking, generate large amounts of carbonaceous by-products such as coke fines, coal tar, and coke oven gas residues. These materials are typically used as low-grade fuel or discarded, despite containing substantial fixed carbon. Here, we focus on a specific coke oven waste stream (detailed in the Section 2) and develop an upcycling process to convert it into battery-grade graphite. We describe the physical and chemical refinement steps, including high-temperature graphitization, and conduct comprehensive structural and electrochemical characterization. Finally, we compare the electrochemical performance of the upcycled graphite with that of commercial graphite benchmarks and discuss the broader sustainability implications for incorporating such waste-to-resource pathways into the circular carbon economy for LIBs.

2. Materials and Methods

2.1. Materials and Sample Preparation

Raw Pit coke waste was obtained as a powdery carbon byproduct from a steel manufacturing process (coke oven). In the context of the steelmaking industry, the term pit coke refers specifically to the coke waste deposited at the bottom of the coke oven pit during the coking process. This by-product consists of agglomerated carbonaceous residues that accumulate beneath the coke oven chamber, and it is distinguished from other forms of coke waste such as coke dust. Initial proximate analysis (described below) showed the Pit material contains a high fixed carbon content along with some volatile matter and ash (impurities). Figure 1 illustrates the generation site of the raw Pit coke and the overall processing route for preparing the anode material. The raw Pit was first subjected to jaw crushing to break down large aggregates. Subsequently, a jet milling process (using a fluidized bed jet mill (CGS16, Netzsch, Bavaria, Germany)) was applied to pulverize the material and narrow the particle size distribution by removing ultrafine particles. The jet-milled sample is referred to as JM_Pit. Next, JM_Pit was spheroidized using a mechano-fusion type spheroidization mill. This process imparts a more spherical shape to the particles through high-energy collisions, which helps increase tap density and improve coating uniformity when the powder is used in electrode slurries. The spheroidized intermediate sample is denoted S_Pit. Finally, the spheroidized powder was graphitized at high temperature. The graphitization was carried out in an inert atmosphere using a high-temperature furnace (Linn High Therm, Bavaria, Germany) with a ramp rate of 10 °C/min up to the target temperature, and a holding time of 2 h at the peak temperature. We investigated graphitization at 3000 °C; the fully graphitized sample is denoted S_Pit3000. We note that the Pit powder inherently contains some metal impurities (as shown later by XRF analysis), which can act as catalysts for graphitization. No additional catalyst or additive was intentionally introduced. For comparison, a commercial graphite anode (CGA) material was obtained (details in Table S3) and a commercial SiOx anode material was also used for making composite anodes.

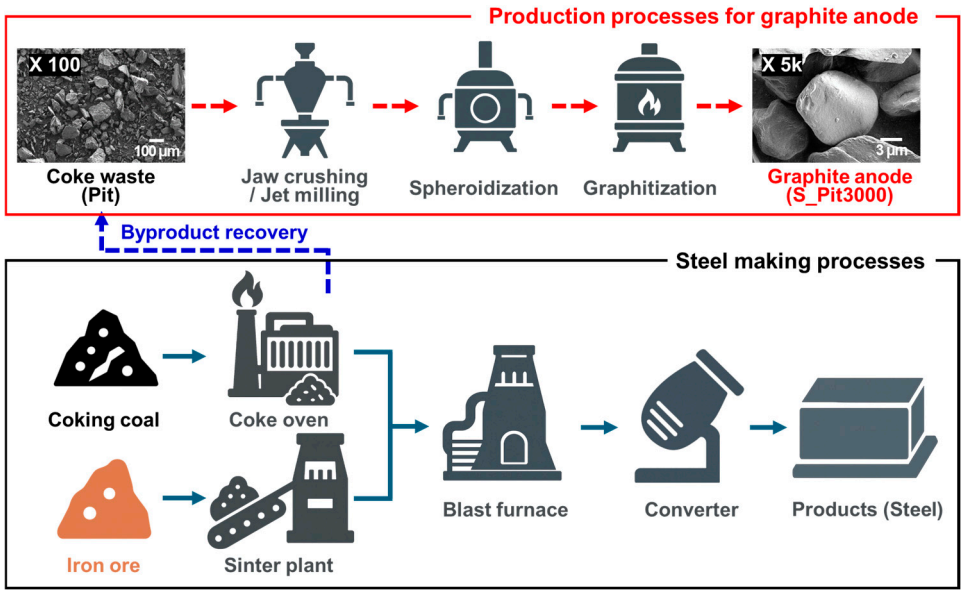

Figure 1. Schematic representation of Pit emission from the steel making process and the subsequent graphite anode production.

2.2. Material Characterizations

Thermogravimetric analysis (TGA701, LECO, St. Joseph, MI, USA) was used to determine the contents of volatile matter, ash (mineral residue), and fixed carbon in accordance with ASTM D2196. These measurements help assess the purity of the carbon material by quantifying non-carbon components (impurities and volatiles).

A laser diffraction particle size analyzer (PSA1090, Anton Paar, Graz, Austria) measured the size distribution of particles (D10, D50, D90 values were obtained). The span of the distribution was calculated as (D90–D10)/D50, with a smaller span indicating a more uniform particle size distribution.

A Dual Autotap density tester (Anton Paar, Graz, Austria) was used to measure tap density, which reflects how densely the powder can pack. Approximately 1–2 g of powder was tapped until volume stabilization, and the mass/volume was recorded.

Nitrogen adsorption–desorption isotherms were measured using a Micromeritics TriStar analyzer (Norcross, GA, USA). The specific surface area was calculated by the BET method. A higher BET surface area generally indicates more porosity or smaller particle size, which can be related to initial electrochemical efficiency.

XRD patterns were collected on a Rigaku D/MAX 2500 VPC diffractometer (Tokyo, Japan) with Cu Kα radiation. Scans were performed from 2θ = 10° to 90° at 0.5°/min. To quantify graphitization, we added 20 wt% of a high-purity silicon standard (Kojundo Chemical, Saitama, Japan) to each sample and normalized peak intensities. The graphitization degree (GD) was calculated by comparing the (002) peak of graphite to the standard, following a literature method. Samples characterized by XRD included raw Pit, JM_Pit, S_Pit, and S_Pit3000.

Scanning electron microscopy (SEM) was performed to observe particle morphology at different stages (using, e.g., a JEOL or FEI SEM at appropriate accelerating voltage). We captured images of raw Pit, milled, spheroidized, and graphitized samples for morphology comparison. Transmission electron microscopy (TEM) was used on the fully graphitized S_Pit3000 to examine the microstructure (lattice fringes, layer spacing) for evidence of crystalline graphitic domains.

For Raman spectroscopy, a RAMANtouch instrument (Nanophoton, Osaka, Japan) was employed, covering the range of 50–3500 cm^{-1}. Raman measurements were conducted using a mapping method over an area of 50 × 50 μm^2.

To analyze the elemental composition of the ash (impurity content), especially from the raw Pit, XRF spectroscopy was used (for example, using a PANalytical or equivalent XRF system). This identified major inorganic components present in the ash after TGA, complementing the proximate analysis.

2.3. Electrode Fabrication

We fabricated CR2032 coin-type half-cells to evaluate the electrochemical performance of the upcycled graphite in a realistic battery setting. For graphite-only anodes, the working electrode slurry was prepared by mixing 96 wt% active material (either S_Pit3000 or commercial graphite as a control), 1 wt% conductive carbon black (Super C65, Imerys) as the conductive additive, and 3 wt% binder (a combination of styrene–butadiene rubber (SBR) and carboxymethyl cellulose (CMC) in a typical 1:1 ratio). Deionized water was used as the solvent to disperse these components, forming a uniform slurry. In the case of composite anodes that include silicon oxide, we blended S_Pit3000 graphite with a commercial SiOx powder. To accommodate the silicon oxide's properties, a small fraction of single-walled carbon nanotubes (SWCNTs) was substituted for a portion of the Super C conductive additive (since SWCNTs can help form a more robust conductive network, beneficial for Si-based anodes). Specifically, SWCNTs replaced ~4.5% of the Super C65 conductive additive, resulting in a conductive additive composition of 0.95 wt% Super C65 and 0.05 wt% SWCNTs in the electrode formulation. The weight ratio of S_Pit3000:SiOx was fixed to 92.2:7.8. After thorough mixing, the slurry was cast onto a copper foil current collector (18 µm thickness) using a doctor blade to control the coating thickness. The coated electrodes were dried at 100 °C for at least 30 min to remove solvent, then roll-pressed to improve density (target electrode density ~1.4–1.6 g/cm^3). The dried, pressed electrodes were punched into 14 mm diameter disks. To ensure removal of any residual moisture, the electrode disks were further dried under vacuum at an elevated temperature (e.g., 120 °C) in a dry room prior to cell assembly.

Figure 2 schematically illustrates the overall process of coin-cell fabrication. Coin cells were assembled in an argon-filled glove box (H_2O < 1 ppm, O_2 < 1 ppm). Each cell consisted of the graphite-based working electrode, a lithium metal counter/reference electrode, a polypropylene separator (Celgard, NC, USA), and a standard carbonate-based electrolyte. The electrolyte used was 1 M $LiPF_6$ salt dissolved in a 30:70 (v/v) mixture of ethylene carbonate (EC) and ethyl methyl carbonate (EMC), which is a common electrolyte formulation providing a good balance of ionic conductivity and solid–electrolyte interphase (SEI) formation on graphite.

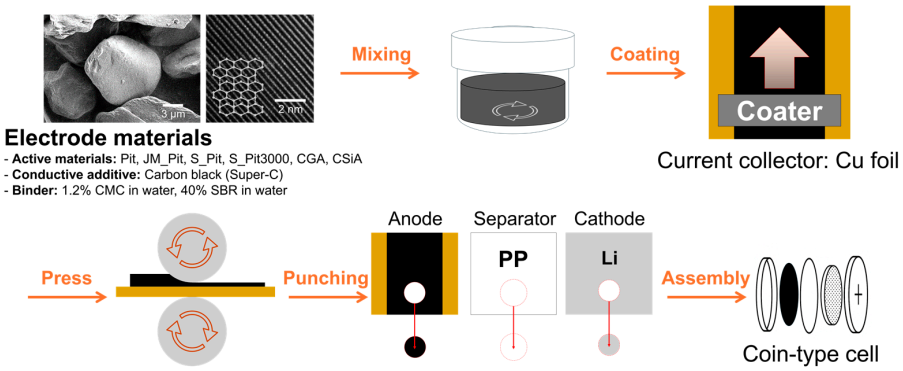

Figure 2. Schematic representation of fabrication of coin-half-cells.

2.4. Electrochemical Measurements

The assembled half-cells were tested using an MRX-MIHW (Neware Laboratories, Guangdong Province, China). Cells were allowed a short rest period after assembly, and their open-circuit voltage (OCV) was measured to confirm proper assembly (typical OCV > 3.0 V for a fresh Li half-cell indicates a functional cell). Galvanostatic charge–discharge cycling was carried out at room temperature. For formation and initial testing, we used a C/10 rate (0.1 C, where 1 C is defined as the current to fully charge in 1 h based on a theoretical capacity of 350 mAh/g for artificial graphite). Cells were cycled between 0.005 V and 1.5 V vs. Li/Li^+ for at least three cycles. The first-cycle charging (lithium insertion in the graphite, also called the formation cycle) was done at 0.1 C to form a stable SEI. We recorded the initial Coulombic efficiency (ICE), calculated as the ratio of the first discharge capacity (lithium extraction, delithiation) to the first charge capacity (lithium insertion) multiplied by 100%. A higher ICE indicates less irreversible capacity loss to SEI formation. Unless otherwise noted, the specific capacities reported are from the third discharge cycle, by which time the cell is assumed to be stabilized and representative of reversible capacity. For the composite anodes containing SiOx, similar cycling protocols were followed, but note that voltage was still limited to 1.5 V vs. Li to avoid extended high-voltage delithiation (since SiOx generally operates in a similar voltage window as graphite with some additional features around 0.5 V).

3. Results and Discussion

3.1. Chemical Purity and Composition of Pit-Derived Carbon

The primary objective of our process is to refine steelmaking coke waste into battery-grade graphite, which requires high carbon purity and minimal impurities [28]. To evaluate the starting Pit material, we performed proximate analysis using TGA. Figure 3a–c shows the TGA-derived composition of the raw Pit: the volatile matter content is about 7.00%, ash (inorganic residue) is 0.10%, and fixed carbon is 92.90%. The high fixed carbon and low 0.1% ash are promising.

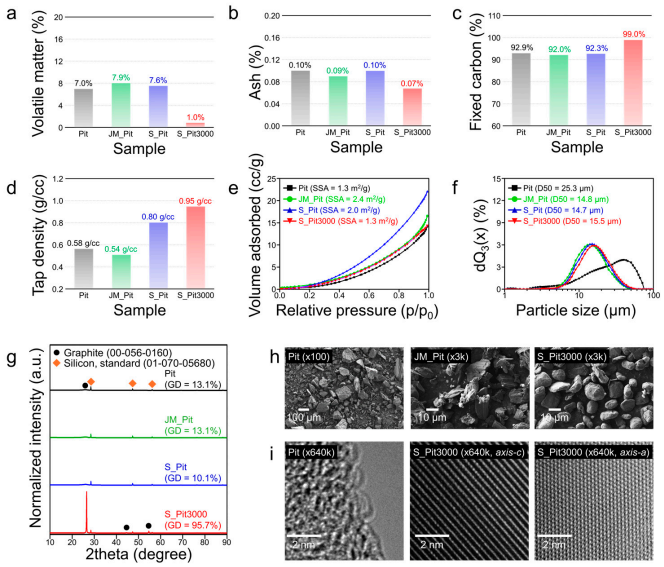

Figure 3. Results of material characterization of Pit, JM_Pit, S_Pit, and S_Pit3000 Using a TGA analysis: (**a**) volatile matter, (**b**) ash, (**c**) fixed carbon. (**d**) Tap Density. (**e**) N_2 adsorption–desorption isotherms indicating specific surface area and pore structure. (**f**) Particle size distributions showing the effect of spheroidization and milling processes. (**g**) XRD patterns confirming the degree of crystallinity and graphitization. (**h**) SEM and (**i**) TEM images illustrating morphological evolution and lattice fringes along specific crystallographic directions.

We found that the jet milling and spheroidization steps did not significantly change the overall chemical composition of the carbon. This is important as it indicates that purely physical processing (size reduction and shaping) does not remove the residual impurities. Thus, to achieve battery-grade purity, a high-temperature treatment is necessary to gasify volatile components into the carbon structure. The consistency of the TGA results from raw Pit through JM_Pit and S_Pit confirms that additional purification (aside from milling) is required to reach the purity needed for LIB anodes. High-temperature graphitization in an inert atmosphere can effectively reduce volatile content such as SO_3 (Table S1).

3.2. Effects of Jet Milling and Spheroidization on Particle Size, Morphology, and Tap Density

Besides purity, particle size and morphology are critical for anode materials. If particles are too large, they may cause poor electrode processing and mechanical issues; if too fine, they lead to excessive surface area and side reactions, lowering initial Coulombic efficiency. We measured the particle size distributions (PSDs) and found significant improvements through our process (see Table S2 for summary data). The raw Pit had a broad size distribution with a D50 (median diameter) of 25.3 μm and a span of 1.72, indicating a wide mix of particle sizes. After jet milling (JM_Pit), the D50 decreased to 14.8 μm, and the span narrowed to 1.22. This narrower distribution means fewer extremely large or ultrafine particles, which is beneficial: it removes oversized particles that could impede slurry casting and very fine particles that increase surface area unnecessarily. Jet milling effectively eliminated the ultrafine fraction (dust-like particles), yielding a more uniform and controlled PSD.

However, jet milling alone produced more angular, flaky particles (typical of milled coke), which is reflected in the relatively low tap density (TD) of JM_Pit (only 0.54 g/cm^3). In LIB anodes, tap density is crucial because a higher tap density allows packing more active material into a given volume, thereby increasing the electrode's volumetric energy density [29–32]. Particle shape heavily influences TD: flake or needle-like particles pack inefficiently, whereas spherical particles pack densely. Therefore, we introduced the spheroidization step to modify particle shape. The spheroidized sample (S_Pit) shows markedly different morphology (SEM images in Figure 3h): large asperities are smoothed out and particles become more rounded after intensive mechanical collisions. Consequently, the tap density of S_Pit increased significantly to 0.80 g/cm^3 (Figure 3d), a ~48% improvement over JM_Pit. Importantly, this increase was achieved without altering the particle size distribution (the D50 and span of S_Pit remained similar to JM_Pit, as shown in Figure 3f and Table S2). This indicates that spheroidization mainly changed particle shape and surface texture, rather than causing further size reduction or classification.

A high tap density also correlates with better slurry coating uniformity and electrode mechanical stability—denser particles settle less and form more robust electrodes when dried and pressed. Thus, the spheroidization step is confirmed to be a critical process for transforming petroleum coke into a morphology suitable for battery electrode fabrication.

We also measured the Brunauer–Emmett–Teller (BET) surface area for the samples. The raw Pit had a relatively high BET surface area (indicative of porous or fine particles). JM_Pit and S_Pit still exhibited quite high surface areas (on the order of a few square meters per gram, data in Table S2), meaning there remained many micro- and nanopores or very small particles contributing to surface area. In LIBs, an excessively large surface area is detrimental as it leads to more solid–electrolyte interphase (SEI) formation and irreversible lithium consumption [33,34]. After the high-temperature graphitization step (3000 °C), the surface area of S_Pit3000 dropped substantially (with N_2 adsorption–desorption isotherms in Figure 3e showing a decrease in gas uptake). This is likely due to the healing of defects/pores and growth of crystalline domains at high temperature, which

effectively "closures" some microporosity. The BET surface area reduction, combined with the spheroidized morphology, is expected to improve the initial Coulombic efficiency in electrochemical testing, as fewer sites are available for SEI to form on the first cycle. In summary, the multi-step physical refinement successfully optimized the particle size (to ~15 μm median, uniformly distributed), shape (spherical), and packing density (~0.8 g/cc), while the final high-temperature treatment improved purity and reduced surface area. Each of these improvements addresses a specific limitation of raw Pit carbon, preparing it for use in LIB anodes.

3.3. Crystallinity Enhancement

Graphitic crystallinity is a critical determinant of anode performance. A well-ordered graphitic structure with large crystalline domains facilitates efficient lithium-ion intercalation, enhances electrical conductivity, and reduces the accessible surface area for undesirable side reactions, thereby ICE and cycle life [35,36]. The degree of graphitic order at each processing stage was quantified using X-ray diffraction (XRD). As shown in Figure 3g, the raw Pit, JM_Pit, and S_Pit samples exhibit broad, weak diffraction peaks near $2\theta \approx 26^{\circ}$, corresponding to the graphite (002) plane, which indicates a predominantly amorphous or turbostratic carbon structure. To ensure quantitative comparison, we added an equal amount (20 wt%) of high-purity silicon (Si) as an internal standard to all samples and normalized the XRD peak intensities with respect to the Si signal. For this reason, the Y-axis scaling in the main figure was kept consistent across samples. Nevertheless, to provide clearer visibility of the (002) peaks of Pit, JM_Pit, and S_Pit, we have additionally included re-plotted XRD patterns with adjusted Y-axis scales in the Supplementary Information (Figure S2). The calculated graphitization degrees (GD) for these samples were in the range of ~10–15%, consistent with non-graphitized coke-derived carbons. In contrast, the S_Pit3000 sample—subjected to 3000 °C heat treatment—displayed sharp, intense diffraction peaks, especially the (002) reflections, signifying a highly ordered graphite lattice. The GD for S_Pit3000 reached ~95.7%, confirming that the majority of the carbon had been transformed into well-crystallized graphite.

TEM provided direct real-space evidence of this transformation (Figure 3i). In the raw Pit (and similarly in pre-graphitized S_Pit), the images show largely disordered carbon with few or no discernible lattice fringes; any fringes present were short, curved, and indicative of small, misoriented graphitic domains. By contrast, S_Pit3000 exhibited long, parallel lattice fringes corresponding to the graphite interlayer spacing of ~0.335 nm, characteristic of the (002) planes. These fringes extended over tens of nanometers, indicating large crystalline domains. Occasional fringes along the a-axis direction were also observed, suggesting substantial in-plane crystalline order in addition to interlayer alignment.

Additionally, to further investigate the defect density and structural ordering of the recycled graphite anodes, we performed Raman spectroscopy measurements at different processing stages (Figure S3). The obtained I_D/I_G ratios were 0.40 (Pit), 0.44 (JM_Pit), 0.42 (S_Pit), and 0.30 (S_Pit3000). The markedly sharper D and G peaks, together with the appearance of a distinct 2D band in S_Pit3000, clearly indicate a higher degree of graphitic ordering compared to the other samples. These findings are consistent with the XRD (Figure 3g) and TEM (Figure 3i) results and further validate the improved structural quality of the upcycled graphite.

This dramatic crystallinity enhancement—from GD ~13% to 95.7%—has clear implications for electrochemical performance. Highly graphitized carbons possess fewer structural defects and lower concentrations of lithium-trapping sites, which reduces irreversible capacity loss associated with SEI formation. Furthermore, the improved crystalline ordering promotes faster Li^+ diffusion along graphitic planes and increases bulk electronic conduc-

tivity, leading to reduced polarization and improved rate capability during cycling. These characteristics suggest that S_Pit3000 should deliver electrochemical behavior comparable to that of commercial graphite, a hypothesis validated in the subsequent electrochemical evaluation. Importantly, the entire upcycling process, including the graphitization step, was achieved without the use of corrosive chemical treatments, offering a more environmentally benign alternative to conventional artificial graphite production methods.

3.4. Electrochemical Performance of Upcycled Graphite Anodes

Finally, we evaluated the electrochemical performance of the refined Pit-derived graphite in half-cell configurations. We compare S_Pit3000 with a commercial artificial graphite anode (CGA) as a baseline. Additionally, we assess a composite anode where S_Pit3000 is blended with SiOx to boost capacity (composite high-capacity anode). The cycling profiles and key metrics are summarized in Figure 4 and Table S4.

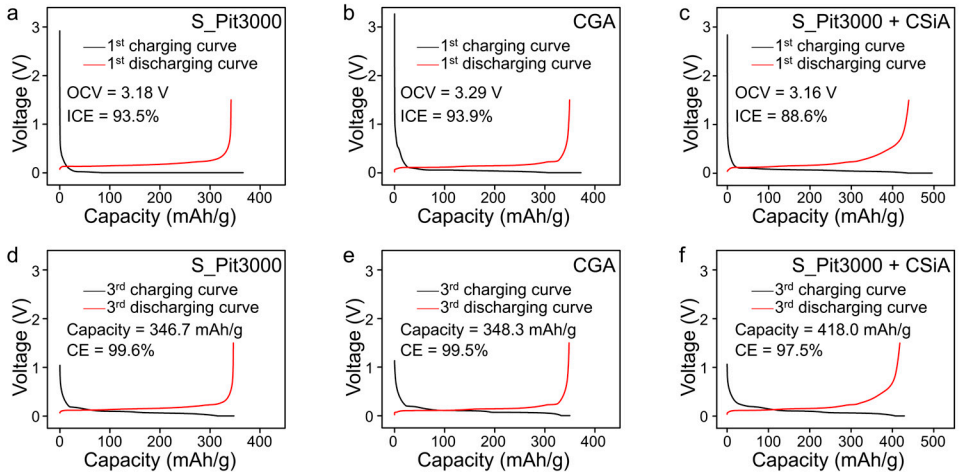

Figure 4. Electrochemical performances of (**a**,**d**) S_Pit3000, (**b**,**e**) CGA, and (**c**,**f**) S_Pit3000 + SiOx composite. Panels (**a**–**c**) show the initial charge–discharge voltage profiles, while panels (**d**–**f**) present the corresponding cycling performance. The initial Coulombic efficiencies (ICE) were 93.5% for S_Pit3000, 93.9% for CGA, and 88.6% for the S_Pit3000 + SiOx composite. In addition, the calculated Coulombic efficiencies (CE) are directly labeled in panels (**d**–**f**): 99.6% (S_Pit3000), 99.5% (CGA), and 97.5% (S_Pit3000 + SiOx composite), confirming stable reversibility of lithium-ion storage.

All cells were first checked for open-circuit voltage, which was >3.0 V, confirming proper assembly (Table S5). Figure 4a,b shows the initial charge–discharge voltage profiles for the graphite-only anodes. S_Pit3000 displays the characteristic voltage plateau of graphite around 0.1 V vs. Li^+/Li during lithiation, corresponding to lithium intercalation into graphitic layers. The shape of the curve (flat plateau and sloping regions) closely matches that of the commercial graphite, reflecting a similar Li^+ insertion profiled characterized by distinct staging phenomena. This statement is supported by previous studies reporting that graphite stores lithium mainly through a reversible staging mechanism without undergoing bulk phase transformations, which differentiates it from many metal-based cathode materials that typically experience structural phase changes during cycling. On the first cycle, S_Pit3000 achieves a charge capacity of 371 mAh/g with a first discharge capacity of 347.0 mAh/g, yielding an ICE of 93.5%. This high ICE is on par with commercial graphite (which showed 93.9% under the same conditions, with a first discharge capacity ~348 mAh/g). Such an ICE (>93%) is a strong indicator that the surface area of S_Pit3000 is low and the SEI formation is moderate, as intended by our processing (indeed, artificial graphite anodes typically have ICE in the 90–94% range when optimized). The slight

irreversible loss (~6.5%) likely corresponds to SEI formation, which is expected even in highly pure graphite.

By the third cycle, S_Pit3000 delivers a reversible discharge capacity of 346.7 mAh/g, very close to that of the commercial graphite anode (348.3 mAh/g). Essentially, within experimental error, the upcycled graphite matches the commercial product in capacity. The charge–discharge curves of S_Pit3000 in the third cycle overlap almost exactly with those of the commercial graphite (Figure 4d,e), demonstrating excellent reversibility and structural stability during the initial cycles. This result validates that our upcycling process can produce graphite capable of sustaining lithium intercalation/deintercalation with performance on par with an established battery-grade material.

We then challenged the material by creating a SiOx-composite anode. Silicon-based anodes can store much more lithium than graphite, but they suffer from volume changes and low initial efficiency. A common approach in industry is to use a silicon oxide (SiOx) or silicon-graphite composite to boost capacity while maintaining good cycling from the graphite component [3,4]. We mixed a portion of commercial SiOx into S_Pit3000 and made composite electrodes. The presence of SiOx (which has a theoretical capacity ~1400 mAh/g but first-cycle inefficiency due to irreversible Li_2O/Li_2Si formation) led to a lower ICE of 88.6% for the composite—this is expected, as SiOx typically has ICE in the 70–80% range on its own. Even so, the composite anode delivered a third-cycle capacity of 418.0 mAh/g, substantially higher than graphite alone. This demonstrates that the Pit-derived graphite can serve as a robust matrix for silicon, accommodating its expansion and benefiting from its high capacity. The fact that our composite's performance is in line with other SiOx-graphite blends used in industry (where ~10% SiOx can raise capacity by 50–100 mAh/g at the expense of 3–5% initial efficiency drop) suggests that the interface between S_Pit3000 and SiOx is favorable and that our graphite has the necessary mechanical stability and surface chemistry to support silicon particles (often, a uniform carbon coating and low impurity content in graphite help in this regard [37]). In addition, the Coulombic efficiencies (CE) of the cells presented in Figure 4d–f were calculated and directly indicated in the figure panels. The CE values were 99.6% for S_Pit3000 (Figure 4d), 99.5% for CGA (Figure 4e), and 97.5% for the S_Pit3000 + SiOx composite (Figure 4f), confirming the stable reversibility of lithium-ion storage in these electrodes [38].

While our electrochemical tests focused on initial cycles and high loading performance, the outcomes are very promising. The upcycled S_Pit3000 graphite meets the key requirements for a LIB anode: high reversible capacity (~350 mAh/g), high initial efficiency (>93%), and compatibility with silicon additives. The close match with commercial graphite performance indicates that despite originating from a waste byproduct, the material, after processing, has essentially been "upgraded" to battery-grade graphite. This is a remarkable result from both economic and environmental standpoints—it suggests that industries could potentially recover carbon from metallurgical waste and use it in batteries, reducing the need for mining or synthetically producing new graphite.

Figure 4 also shows that the voltage profiles of S_Pit3000 remained stable from the first to third cycle, implying that there were no significant side reactions aside from initial SEI formation. For long-term application, a stable SEI and high crystallinity (as S_Pit3000 has) are expected to yield good cycling stability. Although extended cycling and fast-charge tests were beyond the initial scope of this study, they constitute important follow-up work. We anticipate, based on the properties of materials, the S_Pit3000 would exhibit cycle life and rate capability comparable to other artificial graphite samples. Future studies could explore this, as well as optimizations like prelithiation or electrolyte additives to further boost first-cycle efficiency for composite anodes [39–42].

4. Conclusions

In summary, this work successfully demonstrates the upcycling of "Pit" coke oven waste—a previously low-value byproduct of steel manufacturing—into a high-quality graphite anode material for lithium-ion batteries. The multi-step physical refinement process (jet milling, spheroidization, and high-temperature graphitization) proved effective in overcoming the challenges of raw Pit carbon (impurities, poor crystallinity, and irregular morphology) without using any chemical purification. Key improvements in material properties include significantly higher carbon purity (removal of ~7% volatiles and reduction in ash content via graphitization), enhanced particle size uniformity (D50, ~15 μm with narrow distribution), spherical particle morphology (resulting in nearly 50% higher tap density), and near-perfect graphitic crystallinity (~95% graphitization degree for S_Pit3000). These attributes translated directly into excellent electrochemical performance—the upcycled graphite showed an ICE above 93% and reversible capacity ~347 mAh/g, on par with commercial graphite in half-cell tests. Moreover, when used in a composite with SiOx, the material delivered a substantially increased capacity (~418 mAh/g), indicating its suitability as a conductive and resilient matrix for next-generation high-capacity anodes.

Overall, this study provides a scalable and environmentally friendly strategy for producing battery-grade graphite from industrial waste. The approach contributes to waste valorization (adding value to steel industry byproducts) and promotes sustainable materials sourcing for the battery industry, aligning with circular economy principles. By avoiding strong acids or chemical treatments, the process minimizes environmental impact and could potentially be more cost-effective than conventional artificial graphite production.

Supplementary Materials: The following supporting information can be downloaded at https://www.mdpi.com/article/10.3390/batteries11100365/s1. Figure S1. Photographs of commercial anode materials: (left) commercial graphite anode (CGA) and (right) commercial SiOx anode (CSiA). Figure S2. XRD patterns of Pit, JM_Pit, S_Pit samples. Figure S3. Raman spectra of Pit, JM_Pit, S_Pit, and S_Pit3000. The I_D/I_G ratios were determined as 0.40 (Pit), 0.44 (JM_Pit), 0.42 (S_Pit), and 0.30 (S_Pit3000). Table S1. Proximate and X-ray fluorescence analyses of various Pit-derived samples, showing volatile matter, ash, fixed carbon, and elemental compositions. Table S2. Tap density, specific surface area (SSA), particle size distribution, and XRD parameters of Pit-derived samples. Table S3. Specific surface area (SSA), particle size distribution, and electrochemical performance of commercial graphite anode (CGA) and commercial SiOx anode (CSiA). Table S4. CSiA content, loading mass, and electrode density of various Pit-derived samples and commercial anodes. Table S5. CSiA content, open-circuit voltage (OCV), initial coulombic efficiency (I.C.E.), and capacity of Pit-derived samples and commercial anodes.

Author Contributions: Conceptualization, I.Y., S.-M.P. and J.-C.A.; methodology, S.C. and I.Y.; formal analysis, S.C., I.Y., B.L. and T.H.K.; investigation, I.Y. and J.-C.A.; resources, S.C., T.H.K. and S.-M.P.; data curation, I.Y., S.-M.P. and J.-C.A.; writing—original draft preparation, S.C. and I.Y.; writing—review and editing, I.Y., S.-M.P. and J.-C.A.; supervision, S.-M.P. and J.-C.A.; project administration, S.-M.P. and J.-C.A.; funding acquisition, J.-C.A. All authors have read and agreed to the published version of the manuscript.

Funding: This study was supported by "Materials/Parts Technology Development Program (20020300)" funded by the Ministry of Trade, Industry & Energy (MOTIE) of Korea.

Data Availability Statement: The original contributions presented in this study are included in the article/Supplementary Materials. Further inquiries can be directed to the corresponding author(s).

Conflicts of Interest: The authors declare no conflicts of interest.

References

1. Rangarajan, S.S.; Sunddararaj, S.P.; Sudhakar, A.; Shiva, C.K.; Subramaniam, U.; Collins, E.R.; Senjyu, T. Lithium-ion batteries—The crux of electric vehicles with opportunities and challenges. *Clean. Technol.* **2022**, *4*, 908–930. [CrossRef]
2. Bajolle, H.; Lagadic, M.; Louvet, N. The future of lithium-ion batteries: Exploring expert conceptions, market trends, and price scenarios. *Energy Res. Soc. Sci.* **2022**, *93*, 102850. [CrossRef]
3. Promi, A.; Meyer, K.; Ghosh, R.; Lin, F. Advancing electric mobility with lithium-ion batteries: A materials and sustainability perspective. *MRS Bull.* **2024**, *49*, 697–707. [CrossRef]
4. Xu, J.; Cai, X.; Cai, S.; Shao, Y.; Hu, C.; Lu, S.; Ding, S. High-energy lithium-ion batteries: Recent progress and a promising future in applications. *Energy Environ. Mater.* **2023**, *6*, e12450. [CrossRef]
5. Gao, Y.; Pan, Z.; Sun, J.; Liu, Z.; Wang, J. High-energy batteries: Beyond lithium-ion and their long road to commercialisation. *Nano-Micro Lett.* **2022**, *14*, 94. [CrossRef]
6. Ma, X.; Chen, M.; Chen, B.; Meng, Z.; Wang, Y. High-performance graphite recovered from spent lithium-ion batteries. *ACS Sustain. Chem. Eng.* **2019**, *7*, 19732–19738. [CrossRef]
7. Zhao, L.; Ding, B.; Qin, X.; Wang, Z.; Lv, W.; He, Y.; Yang, Q.; Kang, F. Revisiting the roles of natural graphite in ongoing lithium-ion batteries. *Adv. Mater.* **2022**, *34*, 2106704. [CrossRef]
8. Natarajan, S.; Aravindan, V. An urgent call to spent LIB recycling: Whys and wherefores for graphite recovery. *Adv. Energy Mater.* **2020**, *10*, 2002238. [CrossRef]
9. Tian, H.; Graczyk-Zajac, M.; Kessler, A.; Weidenkaff, A.; Riedel, R. Recycling and reusing of graphite from retired lithium-ion batteries: A Review. *Adv. Mater.* **2024**, *36*, 2308494. [CrossRef]
10. Park, J.; Cho, S.-J.; Shin, S.; Kim, R.; Shin, D.; Shin, Y. Overview of graphite supply chain and its challenges. *Geosci. J.* **2025**, *29*, 329–341. [CrossRef]
11. Pol, V.G. Lithium-ion battery critical materials sustainability. *ACS Energy Lett.* **2025**, *10*, 2553–2558. [CrossRef]
12. Bhuwalka, K.; Ramachandran, H.; Narasimhan, S.; Yao, A.; Frohmann, J.; Peiseler, L.; Chueh, W.; Boies, A.; Davis, S.J.; Benson, S. Securing the supply of graphite for batteries. *arXiv* **2025**, arXiv:2503.21521. [CrossRef]
13. Gulley, A.L. The development of China's monopoly over cobalt battery materials. *Min. Econ.* **2024**, *37*, 619–631. [CrossRef]
14. Ellingsen, L.A.; Majeau-Bettez, G.; Singh, B.; Srivastava, A.K.; Valøen, L.O.; Strømman, A.H. Life cycle assessment of a lithium-ion battery vehicle pack. *J. Ind. Ecol.* **2014**, *18*, 113–124. [CrossRef]
15. Moradi, B.; Botte, G.G. Recycling of graphite anodes for the next generation of lithium ion batteries. *J. Appl. Electrochem.* **2016**, *46*, 123–148. [CrossRef]
16. Roy, J.J.; Rarotra, S.; Krikstolaityte, V.; Zhuoran, K.W.; Cindy, Y.D.; Tan, X.Y.; Carboni, M.; Meyer, D.; Yan, Q.; Srinivasan, M. Green recycling methods to treat lithium-ion batteries E-waste: A circular approach to sustainability. *Adv. Mater.* **2022**, *34*, 2103346. [CrossRef] [PubMed]
17. Wang, J.; Ma, J.; Zhuang, Z.; Liang, Z.; Jia, K.; Ji, G.; Zhou, G.; Cheng, H.-M. Toward direct regeneration of spent lithium-ion batteries: A next-generation recycling method. *Chem. Rev.* **2024**, *124*, 2839–2887. [CrossRef] [PubMed]
18. Markey, B.; Zhang, M.; Robb, I.; Xu, P.; Gao, H.; Zhang, D.; Holoubek, J.; Xia, D.; Zhao, Y.; Guo, J.; et al. Effective upcycling of graphite anode: Healing and doping enabled direct regeneration. *J. Electrochem. Soc.* **2020**, *167*, 160511. [CrossRef]
19. Ferdous, A.R.; Shah, S.S.; Shah, S.N.A.; Johan, B.A.; Al Bari, A.; Aziz, A. Transforming waste into wealth: Advanced carbon-based electrodes derived from refinery and coal by-products for next-generation energy storage. *Molecules* **2024**, *29*, 2081. [CrossRef]
20. Lower, L.; Dey, S.C.; Vook, T.; Nimlos, M.; Park, S.; Sagues, W.J. Catalytic graphitization of biocarbon for lithium-ion anodes: A minireview. *ChemSusChem* **2023**, *16*, e202300729. [CrossRef]
21. Zhang, M.; Qu, M.; Yuan, W.; Mu, J.; He, Z.; Wu, M. Green synthesis of hierarchically porous carbon derived from coal tar pitch for enhanced lithium storage. *Batteries* **2023**, *9*, 473. [CrossRef]
22. Lee, G.; Lee, M.E.; Kim, S.-S.; Joh, H.-I.; Lee, S. Efficient upcycling of polypropylene-based waste disposable masks into hard carbons for anodes in sodium ion batteries. *J. Ind. Eng. Chem.* **2022**, *105*, 268–277. [CrossRef]
23. Ji, Y.; Palmer, C.; Foley, E.; Giovine, R.; Yoshida, E.; Sebti, E.; Patterson, A.; McFarland, E.; Clément, R. Valorizing the carbon byproduct of methane pyrolysis in batteries. *Carbon* **2023**, *204*, 26–35. [CrossRef]
24. Hong, S.; Ku, J.; Park, S.; Park, J.; Yu, Y.-S.; Kim, C. Recycling of polyethylene via hydrothermal carbonization for the Li-ion battery anode. *Carbon. Lett.* **2024**, *34*, 1529–1536. [CrossRef]
25. Gharpure, A.; Kowalik, M.; Wal, R.L.V.; van Duin, A.C. Upcycling plastic waste into graphite using graphenic additives for energy storage: Yield, graphitic quality, and interaction mechanisms via experimentation and molecular dynamics. *ACS Sustain. Chem. Eng.* **2024**, *12*, 4565–4575. [CrossRef]
26. Kim, K.S.; Hwang, J.U.; Im, J.S.; Lee, J.D.; Kim, J.H.; Kim, M.I. The effect of waste PET addition on PFO-based anode materials for improving the electric capacity in lithium-ion battery. *Carbon Lett.* **2020**, *30*, 545–553. [CrossRef]
27. Kim, J.-J.; Lee, S.-H.; Roh, J.-S. Effect of heat-treatment temperature and residence time on microstructure and crystallinity of mesophase in coal tar pitch. *Carbon. Lett.* **2024**, *34*, 815–825. [CrossRef]

28. Rong, T.; Guan, W.; Song, W.; Zuo, H.; Wang, J.; Xue, Q.; Jiao, S. Electrochemical graphitization transformation of deposited carbon for Li-ion storage: Sustainable energy utilization from coke oven solid waste. *J. Mater. Chem. A* **2023**, *11*, 84–94. [CrossRef]
29. Zhan, R.; Wang, X.; Chen, Z.; Seh, Z.W.; Wang, L.; Sun, Y. Promises and challenges of the practical implementation of prelithiation in lithium-ion batteries. *Adv. Energy Mater.* **2021**, *11*, 2101565. [CrossRef]
30. He, W.; Guo, W.; Wu, H.; Lin, L.; Liu, Q.; Han, X.; Xie, Q.; Liu, P.; Zheng, H.; Wang, L.; et al. Challenges and recent advances in high capacity Li-rich cathode materials for high energy density lithium-ion batteries. *Adv. Mater.* **2021**, *33*, 2005937. [CrossRef]
31. Li, J.; Fleetwood, J.; Hawley, W.B.; Kays, W. From materials to cell: State-of-the-art and prospective technologies for lithium-ion battery electrode processing. *Chem. Rev.* **2021**, *122*, 903–956. [CrossRef]
32. Bryntesen, S.N.; Strømman, A.H.; Tolstorebrov, I.; Shearing, P.R.; Lamb, J.J.; Burheim, O.S. Opportunities for the state-of-the-art production of LIB electrodes—A review. *Energies* **2021**, *14*, 1406. [CrossRef]
33. Sun, L.; Liu, Y.; Wu, J.; Shao, R.; Jiang, R.; Tie, Z.; Jin, Z. A review on recent advances for boosting initial coulombic efficiency of silicon anodic lithium ion batteries. *Small* **2022**, *18*, 2102894. [CrossRef]
34. Tang, Z.; Zhou, S.; Huang, Y.; Wang, H.; Zhang, R.; Wang, Q.; Sun, D.; Tang, Y.; Wang, H. Improving the initial coulombic efficiency of carbonaceous materials for Li/Na-ion batteries: Origins, solutions, and perspectives, Electrochem. *Energy Rev.* **2023**, *6*, 8. [CrossRef]
35. Xie, G.; Tan, X.; Shi, Z.; Peng, Y.; Ma, Y.; Zhong, Y.; Wang, F.; He, J.; Zhu, Z.; Cheng, X.; et al. SiOx based anodes for advanced Li-ion batteries: Recent progress and perspectives. *Adv. Funct. Mater.* **2025**, *35*, 2414714. [CrossRef]
36. He, W.; Xu, W.; Li, Z.; Hu, Z.; Yang, J.; Qin, G.; Teng, W.; Zhang, T.; Zhang, W.; Sun, Z.; et al. Structural design and challenges of micron-scale silicon-based lithium-ion batteries. *Adv. Sci.* **2025**, *12*, 2407540. [CrossRef]
37. Xiong, Y.; Xing, H.; Fan, Y.; Wei, Y.; Shang, J.; Chen, Y.; Yan, J. SiOx-based graphite composite anode and efficient binders: Practical applications in lithium-ion batteries. *RSC Adv.* **2021**, *11*, 7801–7807. [CrossRef] [PubMed]
38. Liu, X.; Yin, L.; Ren, D.; Wang, L.; Ren, Y.; Xu, W.; Lapidus, S.; Wang, H.; He, X.; Chen, Z.; et al. In situ observation of thermal-driven degradation and stability in graphite anodes. *Nat. Commun.* **2021**, *12*, 4158. [CrossRef]
39. Zhou, Y.; Wang, P.; Wang, K.; Fang, X.; Li, W.; Nai, J.; Liu, Y.; Wang, Y.; Zou, S.; Yuan, H.; et al. Developing high-performance anode-free lithium batteries: Challenges, strategies, and opportunities. *Adv. Funct. Mater.* **2025**, *35*, 2424022. [CrossRef]
40. Natarajan, S.; Divya, M.L.; Aravindan, V. Should we recycle the graphite from spent lithium-ion batteries? The untold story of graphite with the importance of recycling. *J. Energy Chem.* **2022**, *71*, 351–369. [CrossRef]
41. Cameán, I.; Lavela, P.; Tirado, J.L.; García, A. On the electrochemical performance of anthracite-based graphite materials as anodes in lithium-ion batteries. *Fuel* **2010**, *89*, 986–991. [CrossRef]
42. Lee, S.E.; Kim, J.H.; Lee, Y.-S.; Bai, B.C.; Im, J.S. Effect of crystallinity and particle size on coke-based anode for lithium ion batteries. *Carbon Lett.* **2021**, *31*, 911–920. [CrossRef]